ACS APPLIED MATERIALS & INTERFACES

Research Article

www.acsami.org

Highly Efficient and Air Stable Inverted Polymer Solar Cells Using LiF-Modified ITO Cathode and MoO_3/AgAl Alloy Anode

Xiangkun Jia,[†] Ziyao Jiang,[†] Xiaohong Chen,*[,†] Jianping Zhou,[‡] Likun Pan,[†] Furong Zhu,[§] Zhuo Sun,[†] and Sumei Huang[†]

[†]Engineering Research Center for Nanophotonics and Advanced Instrument, Ministry of Education, and Department of Physics, East China Normal University, Shanghai 200062, China

[‡]School of Automation Engineering, Shanghai University of Electric Power, Shanghai 200090, China

[§]Department of Physics, Institute of Advanced Materials, and Institute of Research and Continuing Education (Shenzhen), Hong Kong Baptist University, Kowloon Tong, Hong Kong

Supporting Information

ABSTRACT: The performance and air stability of inverted polymer solar cells (PSCs) were greatly improved using a combination of LiF-modified ITO cathode and a MoO_3/AgAl alloy anode. The power conversion efficiency (PCE) of PSCs with AgAl contact reached 9.4%, which is higher than that of the cells with Ag (8.8%) and Al electrode (7.6%). The PCE of AgAl-based PSCs can further increase up to 10.3% through incorporating an ultrathin LiF-modified ITO. AgAl-based cells also exhibit a superior stability compared to the cells with Ag and Al contacts. PCE of the AgAl-based cells without encapsulation remains 78% of its original value after the cells were aged for 380 days in air. The presence of a LiF-modified ZnO interlayer between ITO and the organic active layer improves the charge collection. The improvement in PCE and stability of the AgAl-based cells is primarily attributed to the formation of AlO_x at the MoO_3/AgAl interface, preventing Ag diffusion and improving the built-in potential across the active layer in the cells.

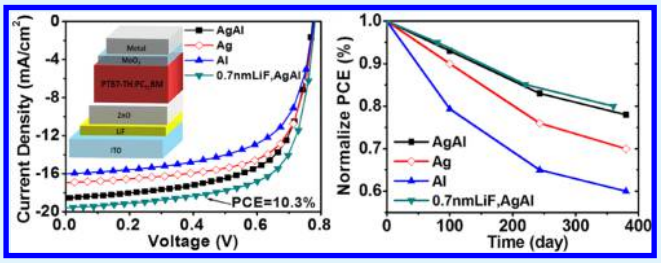

KEYWORDS: *polymer solar cells, AgAl alloy, high efficiency, LiF interlayer, stability, electrodes, ZnO, MoO_3*

1. INTRODUCTION

Bulk heterojunction polymer solar cells (PSCs) have attracted great attention as a promising alternative photovoltaic technology because of their solution-based fabrication process, lightweight and large-scale production at low cost.[1−5] PSCs have enjoyed significant progress over the past decade, with power conversion efficiency (PCE) of single junction PSCs exceeding 10%[5−8] and 12%[9] for triple-junction PSCs. The progress in low band gap polymer with deep highest occupied molecular orbital (HOMO) energy level helped to improve the short circuit photocurrent (J_{SC}) and open circuit voltage (V_{OC}) of the cells. PSCs with an inverted structure are usually preferred for efficient operation as compared to the regular configuration.[10] Different approaches have been developed to improve the performance of PSCs, including the optimization of the active layer thickness,[7] the control of film morphology,[11−13] inserting an optical spacer layer,[3,14−16] use of the photonic structure and surface plasmonic effect[17,18] to boost the light absorption and modification of electrode and/or interlayer to improve the charge collection efficiency have also been demonstrated. In a recent work, we found that the insertion of a ZnO interlayer between the active layer and the metal contact enables to eliminate the unfavorable exciton dissociation, thereby improving the charge collection efficiency.[19] Among the reported high effective low band gap polymers, the use of representative inverted bulk heterojunction PSCs, e.g., based on poly[4,8-bis(5-(2-ethylhexyl)-thiophen-2-yl)-benzo [1,2-*b*:4,5-*b*′] dithiophene-*alt*-3-fluoro-thieno [3,4-*b*] thiophene-2-carboxylate] (PTB7-Th) and [6,6]-phenyl C_{71}-butyric acid methyl eater ($PC_{71}BM$) blend system, greatly improved the PCE of the cells from ∼8% to ∼10% by introducing, for example, polyelectrolytes, fullerene derivative doped ZnO and InZnO, as a cathode interlayer.[5,20−22]

For conventional PSCs, poly(3,4-ethylenedioxythiophene)/poly(styrenesulfonate) (PEDOT:PSS) coated ITO electrode and low work function metals usually act as an anode and cathode, respectively. The acidic PEDOT:PSS layer is detrimental to the ITO anode[23−25] and the air-sensitive low work function metal cathode is easily oxidized, resulting in quick degradation of PSC after exposure to air. Compared with the regular structure PSCs, the reverse configuration allows for improving the absorption in the active layer in the cells, and therefore the PCE. An improvement in operation stability of the inverted PSCs was demonstrated using an accelerated aging test in air.[26] The inverted PSCs may use a less air-sensitive high

Received: October 26, 2015
Accepted: January 21, 2016
Published: January 21, 2016

DOI: 10.1021/acsami.5b10240
ACS Appl. Mater. Interfaces 2016, 8, 3792−3799

work function metal anode such as Ag and Au, and ZnO or TiO_x as an electron selective interlayer between ITO and the active layer, which apparently inhibits electrode oxidation and prolongs cell lifetime.[27−29] The morphology of the active layer is also related to the lifetime of PSCs, which can be improved by tuning the chemical structure of the polymer[30] and/or the device structure design,[31] such as using the inverted geometry. Solution-processed ZnO nanoparticles due to their relatively high transparency, high electron mobility and air stability are commonly used as a good electron transport/collecting layer in inverted PSCs. However, ZnO-based PSCs usually suffer from serious interfacial recombination due to defect induced recombination at the interface between ZnO and the active layer. Recently, fullerene derivative,[32] conjugated polyelectrolytes[33] and ionic liquid functionalized carbon nanoparticles,[34,35] have been reported to modify a ZnO layer to optimize contact properties between ZnO and a photoactive layer and/or passivate traps of bulk ZnO layer, improving the photocurrent and fill factor of PSCs. Liao et al.[5] reported that PSCs exhibit the improved PCE values from 8.25% to 10.31% using a dual-doped ZnO film, due to improved surface conductivity and enhanced electron mobility. A two-step sputtered ZnO cathode interfacial layer with different O_2/Ar gas ratios can also efficiently improve PCEs of PSCs due to enhancing electron extraction ability and inhibiting the defects of the ZnO layer.[36]

For high performance inverted PSCs, anode interlayer materials with high work functions are needed. It is difficult to form an ohmic contact between the low band gap polymers with a deep HOMO energy level and an air-insensitive high work function metal top anode.[3] The typical transition metal oxides, such as MoO_3, WO_3 and V_2O_5, are *n*-type and often used as the anode interlayer in PSCs. MoO_3 is an excellent hole injection material and can form ohmic contact with many organic hole transporting materials. The work function of MoO_3 also exhibits a strong dependence on the stoichiometry and is sensitive to surface contamination. The work function of MoO_3 decreases from 6.5−6.9 eV to 5.3−5.7 eV upon exposure to oxygen or air.[37] For high efficient PSCs, the optimum HOMO level of the low band gap polymers generally resides between 5.2 and 5.6 eV considering the trade-off relationship between V_{OC} and optical absorption band. Therefore, MoO_3 is a suitable interlayer choice to yield a good ohmic contact with low band gap polymers having a low HOMO energy level of 5.2−5.6 eV. Using MoO_3 as a top anode interlayer, inverted PSCs with air-insensitive high work function metals as an anode have widely been reported.[37−40] Compared to the conventional bottom MoO_3 as an anode interlayer, ohmic contact can be enhanced when MoO_3 and silver are deposited sequentially on organic materials forming a top anode interlayer in inverted PSCs.[37] However, few reports suggest that the performance of inverted PSCs with a MoO_3 anode interlayer is dependent on the anode metals. It is shown that the dope of Al in the MoO_3 layer results in decrease in its work function,[41] which favors the electron injection at the MoO_3/electrode interface. The increase in the concentration of electrons in MoO_3 layer assists in hole extraction from donor polymer.

Al and Ag films have high optical reflectivity and excellent electrical conductivity, and are widely used as metal electrodes in PSCs. The average optical reflectivity of Ag film over the visible light wavelength range is about 97%, which is 10% higher than that of Al film. The absorption in the active layer is limited due to the mismatch between optical absorption length and charge transport scale, caused by the low carrier mobility in the organic semiconductors.[1] The Ag electrode with a higher reflectivity helps to improve the optical absorption in the active layer through the interference effect. However, the diffusion of Ag atoms in the active layer formed during thermal evaporation and aging can deteriorate contact quality at the organic/Ag interface, leading to a decrease in the built-in potential across the active layer and an increase in carrier recombination.[42] AgAl alloy contact can be an ideal electrode for PSCs and has been successfully used for application in solar thermal devices[42] and light emitting diodes.[43,44] Compared to the conventional Ag electrode, AgAl alloy contact is more thermally stable due to the formation of AlO_x on the surface of the AgAl alloy,[44] which acts as a barrier to prevent the diffusion and agglomeration of the Ag atoms.[42,44] The formation of the AlO_x interlayer can also improve the adhesion between AgAl and the active layer, promoting a desired ohmic contact at the organic/electrode interface in PSCs.[45,46] In this work, the effect of different top metal contacts of Al, Ag and AgAl alloy on the performance of the structurally identical inverted PSCs was investigated. The inverted PSCs with AgAl top contact have superior performance compared to that of the cells with Al and Ag top electrodes. The highest PCE of the inverted AgAl-based PSCs is 9.4% and further increases to 10.3% for cells having a cathode contact with an ultrathin LiF-modified ITO contact.

2. EXPERIMENTAL SECTION

PSCs, with a structure of ITO/LiF/ZnO/PTB7-Th:$PC_{71}BM$/MoO_3/top electrode, having different contacts of Al, Ag and AgAl alloy were fabricated. The prepatterned indium tin oxide (ITO)/glass substrates (10 Ω/□) were cleaned sequentially with detergent, deionized water, acetone and isopropyl alcohol in an ultrasonic bath for 20 min each, and then blow-dried by pure nitrogen gas. After being dried in the oven, ITO/glass substrates were treated with ultraviolet ozone for 15 min. The sol−gel ZnO nanoparticles were synthesized following the procedures described in previous publications.[18,20,47] In a typical synthesis, a stoichiometric amount of tetramethylammonium hydroxide dissolved in ethanol (0.5 M) was gradually dropped into 0.1 M zinc acetate dihydrate dissolved in dimethyl sulfoxide (DMSO), followed by stirring for 1 h at room temperature. After being washed with hexane and ethanol (2:1) mixing solvents, ZnO nanoparticles were dispersed in ethanol. Then sol−gel ZnO solutions were spin coated at 4000 rpm for 50 s onto ITO to form 20 nm films, followed by annealing at 150 °C for 30 min in air. PTB7-Th (99%) was purchased from 1-Material INC. and $PC_{71}BM$ (99.5%) was purchased from Solenne BV. An 80 nm thick active layer was deposited on the ZnO surface using a blend solution containing PTB7-Th:$PC_{71}BM$ (7 mg/mL:10.5 mg/mL) dissolved in chlorobenzene/1,8-diiodooctane (97:3, v/v) at 1000 rpm for 15 s in argon-filled glovebox. A 7 nm thick MoO_3 interlayer and a 100 nm thick top contact (Ag, Al and AgAl) were then deposited by thermal evaporation at the rate of 0.3 and 6 Å/s, respectively on the PTB7-Th:$PC_{71}BM$ active layer with a base pressure of 3×10^{-4} pa. The weight ratio (wt %) of Al to Ag in the AgAl alloy, purchased from Trillion Metals Co., Ltd. (Beijing, China), is 3 wt %. Unless indicated separately, in the following discussion, a AgAl alloy electrode with 3 wt % of Al was used in the cell fabrication. A mask with an aperture area of 0.09 cm^2 was used for the current density−voltage (*J*−*V*) characteristic measurement to avoid the edge effect. The PSCs were stored in a 10% RH chamber in air.

The *J*−*V* characteristics of PSCs were measured by a Keithley 2440 Sourcemeter together with a Newport solar simulator with an AM1.5G illumination of 100 mW/cm^2 calibrated with a standard silicon reference cell. The incident photon to current conversion efficiency (IPCE) of PSCs was measured over the wavelength range from 300 to 800 nm using a Newport Optical Power Meter 2936-R and was recorded using TracQ Basic software. The dark *J*−*V* characteristics of the cells were measured using an electrochemical workstation (AUTOLAB PGSTAT302N). The absorption and reflectivity spectra

DOI: 10.1021/acsami.5b10240
ACS Appl. Mater. Interfaces 2016, 8, 3792−3799

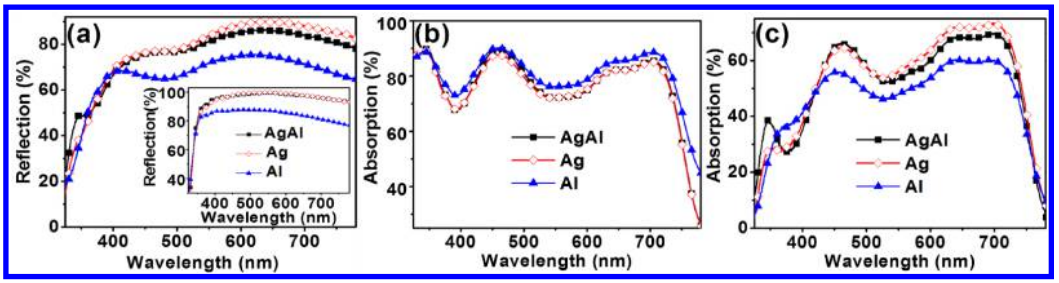

Figure 1. (a) Reflectivity spectra measured for Al, Ag and AgAl films deposited on ITO/glass substrate. Inset in panel a: the reflectivity spectra measured for different metal films deposited on bare glass substrate. (b) Absorption spectra of a set of structurally identical cells of ITO/ZnO/PTB7-Th:$PC_{71}BM$/MoO_3/electrode having different top contacts of AgAl, Ag and Al, (c) absorption spectra of the active layer of the cells made with top electrodes.

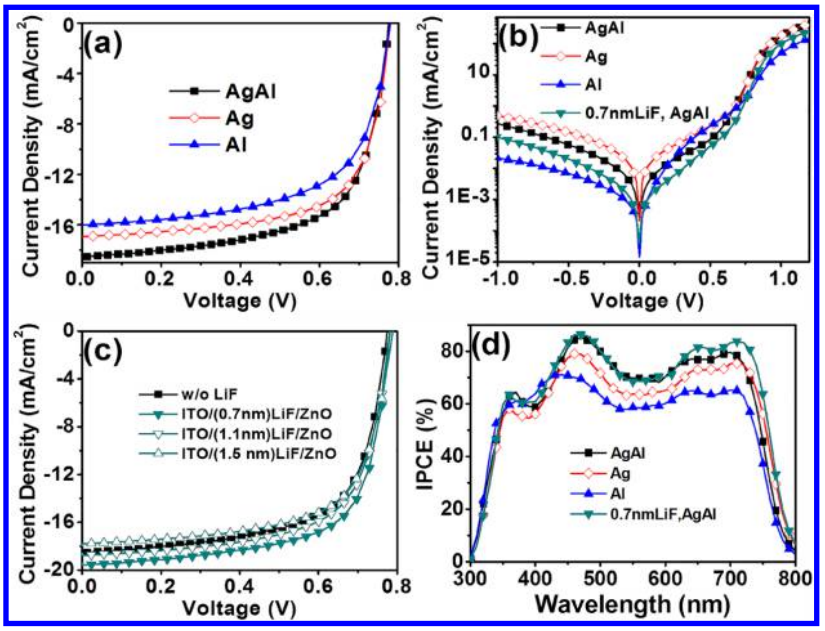

Figure 2. (a) $J-V$ characteristics measured for PSCs with different top electrodes of Ag, Al and AgAl under AM 1.5G illumination of 100 mW/cm^2 and (b) dark condition (b), (c) $J-V$ characteristics of AgAl-based PSCs with different thicknesses of the LiF interlayer interposed between ZnO and ITO. (d) IPCE spectra of PSCs with different electrodes.

of devices with different top contacts of Al, Ag and AgAl were measured using a UV/vis spectrophotometer (Hitachi U-3900). X-ray photoelectron spectroscopy (XPS) measurements were carried out using an Imaging Photoelectron Spectrometer (Axis Ultra, Kratos Analytical Ltd.) with a monochromatic Al Ka X-ray source. The surface morphology of metal films was analyzed using field-emission scanning electron microscopy (FESEM, Hitachi S-4800). The work function values of Ag (4.8 eV), AgAl (4.7 eV) and Al (4.3 eV) contacts in the cells were measured using the Test Instrument of Surface Work Function (Sunmonde Electric Light Source Technology (Shanghai) Co. Ltd.).

3. RESULTS AND DISCUSSION

The high optical reflectivity of an electrode is important to improve the absorption in the active layer of the cells. The reflectivity spectra measured for Al, Ag and AgAl films are shown in Figure 1a. The reflectivity of Ag and AgAl film is apparently higher than that of Al film. The oscillation behavior seen in the reflective spectra of the metal/ITO/glass specimens over the wavelength range from 450 to 500 nm is attributed to the optical interference. The relative stronger reflectivity of Al film at the short wavelength results in more apparent protrusion at the wavelength of 400 nm. Absorption spectra of the cells are shown in Figure 1b. The stronger absorption in Al-based cells is attributed to the lower reflectivity and stronger absorption of Al contact as compared to that of the cells with AgAl and Ag top contacts. The absorption spectra of the PTB7-Th:$PC_{71}BM$ active layer in the cells were obtained by deducting the absorption due to the metal contacts, as shown in Figure 1c. The absorption peak of the active layer in the cells with an Al top contact is slightly blue-shifted from 460 to 452 nm due to the relative higher reflectivity of Al in the short wavelength and optical interference effect, as shown in Figure 1a. The observable lower absorption in the active layer of the cells with Al top contact is ascribed to its relatively lower reflectivity as compared to that of the Ag and AgAl top electrodes. This indicates that the higher reflection Ag and AgAl top electrodes enhance the absorption in the active layer. The similar optical absorption in the PTB7-Th:$PC_{71}BM$ active layer of the cells with Ag and AgAl top contacts are due to the similar reflectivity of AgAl and Ag, suggesting that the difference in the PCE values of the PSCs with Ag and AgAl top electrodes is associated with the variation in the charge collection at the organic/anode interfaces in the cells.

To investigate the effect of different top metal contacts of Ag, Al and AgAl on the performance of inverted PSCs, we fabricated three types of devices with the structure of ITO/

DOI: 10.1021/acsami.5b10240
ACS Appl. Mater. Interfaces 2016, 8, 3792−3799

Table 1. Performance of PSCs, with a Structure of ITO/ZnO/PTB7-Th:$PC_{71}BM$/MoO_3/Electrode, Having Different Top Electrodes of Ag, Al and AgAl

anode	V_{OC} (V)	J_{SC} (mA/cm^2)	*FF* (%)	R_S (Ω·cm^2)	R_{SH} (Ω·cm^2)	*PCE* (%)
Al	0.763	15.0	64.2	43.0	5028.1	7.4 ± 0.2
Ag	0.771	16.7	67.5	37.3	5490.9	8.7 ± 0.1
AgAl	0.780	18.2	66.2	30.0	4739.3	9.3 ± 0.1

Table 2. Performance of AgAl-based PSCs with LiF-Modified ITO Having Different Thicknesses of the LiF Interlayer

	V_{OC} (V)	J_{SC} (mA/cm^2)	*FF* (%)	R_S (Ω·cm^2)	R_{SH} (Ω·cm^2)	*PCE* (%)
without LiF	0.780	18.2	66.2	30.0	4739.3	9.3 ± 0.1
ITO/LiF(0.7 nm)/ZnO	0.782	19.5	67.6	27.4	4102.5	10.3 ± 0.1
ITO/LiF(1.1 nm)/ZnO	0.782	18.8	66.0	33.0	4057.1	9.7 ± 0.1
ITO/LiF(1.5 nm)/ZnO	0.783	17.8	66.0	42.8	5383.4	9.2 ± 0.1

ZnO/PTB7-Th:$PC_{71}BM$/MoO_3/metal electrode. Figure 2a shows the best *J*−*V* characteristics measured for the device with different top contacts. The average device parameters of eight cells made with three top metal contacts, and the standard deviations are summarized in Table 1. The PCE values of the cells with AgAl, Ag and Al top contacts are 9.4%, 8.8% and 7.6%, respectively. The average PCE of cells with a $Ag_{92}Al_8$ (8 wt % Al) top contact is 9.1%, which is still higher than that of cells with Al and Ag top electrodes, as shown in Table S1 in the Supporting Information. The lowest PCE of the PSCs with a AgAl top electrode is 9.2%, which is 5% larger than the best PCE of the cells with a Ag top electrode. The apparently lower J_{SC} of Al-based PSCs, as compared to that of the cells with the Ag and AgAl alloy top electrodes, is attributed to the relative low reflectivity of the Al top contact, resulting in low absorption in the active layer. This argument can further be supported by evaluating the IPCE characteristics of the cells. Figure 2d shows the IPCE curves of PSCs with different metal electrodes. The IPCE peak of cells with Al electrode in the wavelength range from 400 to 500 nm is slightly blue-shifted from 465 to 440 nm compared to cells with Ag and AgAl contacts, in agreement with the blue-shift seen in the absorption spectrum of the active layer with Al electrode, shown in Figure 1c, due to the relative high reflectivity of Al contact in the short wavelength range and its interference effect between glass and Al film. The reduced IPCE values of cells in the wavelength range from 500 to 600 nm are associated with the weak absorption of the PTB7-Th:$PC_{71}BM$ active layer in this wavelength range. This suggests that the absorption enhancement in PTB7-Th:$PC_{71}BM$, due to high optical reflectivity of Ag and AgAl top contacts, contributes to the improvement in PCE of the cells. Considering the slightly different reflectivity of Ag and AgAl films, the enhanced PCE values of cells with AgAl compared to Ag is attributed to the improvement in the contact quality at MoO_3/AgAl interface due to the formation of AlO_x. Because Al atoms are easily diffused out of AgAl alloy and oxidized into AlO_x by the residual oxygen that is absorbed on the cells surface and exists in the vacuum chamber during thermal evaporation.[44] In a previous work, it has been demonstrated that an initial passivation at organic/cathode interface, an inevitable process due to the presence of residual oxygen, moisture and other impurities, is one of the degradation mechanisms.[48] In this work, the serial resistance (R_S) of PSCs with Al electrode decreased from 43.0 to 37.3 Ω·cm^2 for cells with a Ag electrode, and further decreased to 30 Ω·cm^2 for the ones with a AgAl electrode. The reduction in the R_S of cells reveals the decrease in the contact barrier at the MoO_3/AgAl interface, which is beneficial for hole extraction. Furthermore, the dark *J*−*V* characteristics of PSCs with a AgAl electrode, shown in Figure 2b, exhibit better diode characteristics with a lower leakage current and a higher rectification ratio as compared to the cells with a Ag electrode. The reduced leakage current indicates that the formation of AlO_x at the MoO_3/AgAl electrode interface can prevent Ag diffusion and hence reduce the carrier recombination.[42] Al-based cells show the lowest leakage current as compared to the PSCs with AgAl and Ag electrodes, indicating that formation of an AlO_x interlayer plays an important role in reducing the recombination of the carriers at the organic/anode interface. The lower work function of Al electrode (4.3 eV) and the formation of a thicker AlO_x interlayer at the MoO_3/Al interface in Al-based PSCs possibly coinduce a slight decrease in V_{OC} (0.763 eV), caused by an increase in R_S, as shown in Table 1. Therefore, the improvement in PCE of the cells with a AgAl electrode is primarily ascribed to superior contact properties at the interface of MoO_3/AgAl and lower leakage current, as compared to those of the PSCs with just a Ag top electrode.

A solution-processed ZnO interlayer is commonly used as a good electron transport/collection layer in inverted PSCs, due to its high transparency, high electron mobility and air stability. It becomes important to improve the photocurrent and fill factor of PSCs by appropriate modification of the ZnO interlayer to optimize the contact properties at the ZnO/ITO and ZnO/organic interfaces, and to suppress the carrier traps induced by the defects in the ZnO interlayer.[18,34,35] A LiF-modified ITO electrode can lead to a reduction of work function of ITO electrode, which can improve contact quality at the ZnO/ITO interface and help to improve electron extraction in PSCs.[18,49] Therefore, a thin LiF-modified ITO electrode was used to achieve the desired contact at the ZnO/ITO interface and to improve further the PCE of AgAl-based cells. Figure 2c shows the PCE values of AgAl anode-based cells with different thickness of LiF interfaces. Table 2 presents the average values of the cell parameters and their standard deviations measured for the PSCs fabricated with different nominal thickness of LiF layer. The PCE of the PSCs with a 0.7 nm thick LiF interlayer increases from 9.4% to 10.3% for the cells with LiF-modified ITO, which is 15% larger than the PCE (8.8%) of the best performing device with a Ag top electrode. This suggests that incorporating a LiF layer can greatly improve the quality of the ZnO/ITO-based cathode, leading to a decrease in the R_S from 30.0 to 27.4 Ω·cm^2. With further increasing LiF thickness, the thicker LiF layer serves as an insulator resulting in lower J_{SC}, PCE and higher R_S of PSCs.[17,18] Considering the possible

DOI: 10.1021/acsami.5b10240
ACS Appl. Mater. Interfaces 2016, 8, 3792−3799

variation in the thickness of the LiF interlayer during subsequent coating of a ZnO layer by a solution-process (ethanol) approach, the composition of the LiF layer before and after the ethanol solvent treatment was analyzed by XPS measurements (Figure S1). The intensity of the F 1s XPS peaks (at 685 eV) measured for the LiF layer before and after ethanol solvent treatment is almost the same, indicating that the quality of the LiF film was not damaged by the subsequent ZnO thin film fabrication.

To understand further the mechanism responsible for the enhanced performance of cells with a AgAl alloy top contact electrode, we investigated the carrier transport and collection properties in inverted PSCs with different top metal electrodes.[21,22,50] Figure 3a shows the effect of different metal

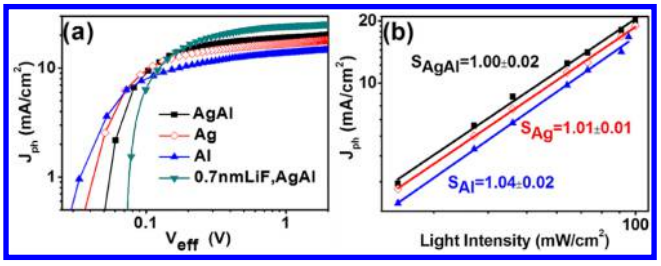

Figure 3. (a) J_{ph}–V_{eff} and (b) J_{ph}–light intensity characteristics measured for PSCs with different top electrodes of AgAl, Ag and Al.

electrodes on the photocurrent density (J_{ph}) of the three cells. J_{ph} is defined as $J_{ph} = J_L - J_D$, where J_L and J_D are the current density under illumination and in the dark, respectively. The effective voltage (V_{eff}) = $V_0 - V_a$, where V_0 is the voltage at which J_{ph} = 0 and V_a is the applied bias voltage. The J_{ph} increases linearly with V_{eff} at low V_{eff} range and gradually saturates at a high V_{eff}. In general, the saturated photocurrent (J_{sat}) is correlated to the maximum exciton generation rate (G_{max}), exciton dissociation probability, and carrier transporting and collection probability at a high V_{eff} region. G_{max} is mainly governed by absorption of light in the active layer. Considering the constant of absorbed incident photons for one cell, assuming that all the photogenerated excitons are dissociated into free charge carriers at a high V_{eff} region, J_{sat} is then limited by the carrier transport and collection. Therefore, carrier transporting and collecting probability at any effective voltage can be obtained directly from the ratio of J_{ph}/J_{sat}. The carrier transporting and collection probabilities of cells with AgAl electrode under the short-circuit condition increased to 88% from 85% for cells with Ag and Al electrodes, and further increased to 91% after using a LiF-modified ITO electrode, indicating that using a MoO_3/AgAl anode and LiF-modified ITO cathode can greatly improves carrier transport and collection of the cells. The J_{ph} values of cells with AgAl, Ag and Al top contacts were varied linearly with light intensity, as shown in Figure 3b, yielding the same power exponent of 1.0. These similar phenomena suggest that the difference in the charge accumulation at the organic/anode interface in cells with different top contacts of AgAl, Ag and Al cannot apparently be distinguished in the range of 10–100 mW/cm^2. Therefore, the improved charge collection in cells with a AgAl top electrode, due to the formation of an AlO_x interlayer as compared to the cell with a Ag electrode, is associated with the suppression of the diffusion of Ag atoms and improvement of the built-in potential across the active layer in the cells, leading to a reduction in the carrier recombination.

Figure 4a shows the normalized PCE of PSCs as a function of aging time. The devices without encapsulation were kept in

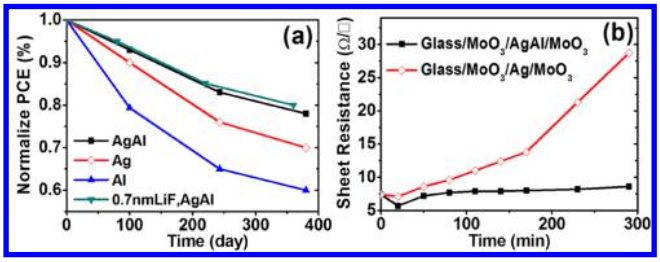

Figure 4. (a) Normalized PCE of PSCs as a function of the aging time. (b) Sheet resistance measured for two thin film stacks of MoO_3/AgAl/MoO_3 and MoO_3/Ag/MoO_3, annealed at 300 °C, as a function of the aging time.

drying cabinet with a relativized humidity of 10% under ambient atmosphere. The PCE of PSCs with AgAl alloy anode remains 78% of the initial PCE value after 380 days of aging test in air, indicating that AgAl alloy electrode has the advantage for improving the performance and stability of cells, which is attributed to the presence of an AlO_x interlayer resulting in forming a thermally stable organic/anode contact in the inverted PSCs, supported by the Auger electron spectroscopy analysis[44] the nonuniform distribution of Al atoms in AgAl and a rich AlO_x layer formed at the interface of AgAl/MoO_3.[44,51] The enhanced adhesion of between the AgAl film and the glass, as compared to that between Ag and glass substrate, shown in Figure S2, was further manifested using an ultrasonic bath in water, supporting the presence of AlO_x. The sheet resistance of the thin film stack of MoO_3/Ag/MoO_3, annealed at 300 °C, increased rapidly after 180 min, as shown in Figure 4b. Whereas that of the MoO_3/AgAl/MoO_3 stack retained a sheet resistance of 8 Ω/□ for more than 300 min under the same annealing condition, indicating that the superior thermal stability of the MoO_3/AgAl/MoO_3, due to the formation of AlO_x that prevents the diffusion and possible aggregation of Ag in the AgAl alloy layer. The observation is consistent with the previous report on enhanced thermal stability of Ag–Al_2O_3 blended film.[52] The suppression of Ag agglomeration in the AgAl layer was further examined using SEM measurements, e.g., the SEM images shown in Figure 5. The SEM image difference between 100 nm thick Ag and AgAl electrodes cannot be obviously distin-

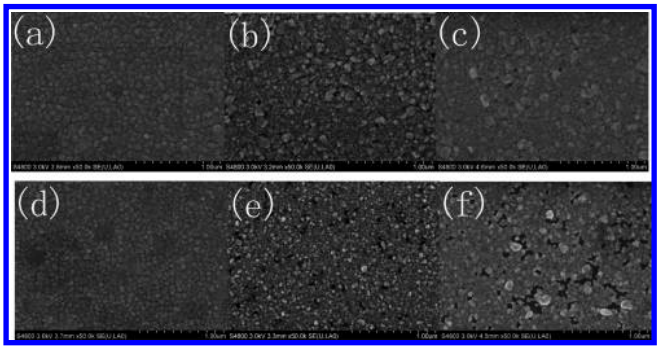

Figure 5. SEM images measured for the PSCs with two different top electrodes of AgAl (a) and Ag (d). SEM images of 12 nm thick AgAl before (b) and after (c), and 12 nm thick Ag before (e) and after (f) annealed at 140 °C for 10 min in argon-filled glovebox. 12 nm thick AgAl and Ag films were thermally evaporated onto the substrate of MoO_3 (7 nm)/glass, respectively.

DOI: 10.1021/acsami.5b10240
ACS Appl. Mater. Interfaces 2016, 8, 3792–3799

guished, as shown in Figure 5a,d. Compared with AgAl, the 12 nm thick Ag film contains more voids and further is aggregated after annealing, indicating that AgAl film shows denser morphology and better stability. The enhanced thermal stability of AgAl films, showing smooth surface as compared to that of the Ag film before and after the same aging test, is clearly demonstrated and is the main reason for forming the high quality organic/anode contact, and therefore prolongs the lifetime of the inverted PSCs.

The cells with LiF-modified ZnO layers usually significantly improve stability of cells compared to cells with bare ZnO layer.[18,20] However, the stability of the cells with AgAl alloy contact and LiF-modified ITO is slightly improved than that of cells without a LiF interlayer, suggesting that LiF film can inhibit the deterioration of the ITO/ZnO interface. Considering the AgAl alloy top electrode and LiF-modified ITO cathode, the slightly enhanced stability of cells with a LiF-modified ITO electrode is possibly attributed to the AlO_x formation at AgAl films that can block moisture diffusion and inhibit the deterioration of the ITO/ZnO interface. Therefore, the enhanced stability role of the LiF interface cannot be reflected completely. Niu et al. reported better stability of cells by inserting an Al_2O_3 layer between perovskite and hole transporting layers due to blocking moisture of Al_2O_3.[53] The $CH_3NH_3PbI_3$ film is sensitive to the moisture and becomes yellow from dark brown under the interaction of moisture because $CH_3NH_3PbI_3$ can be decomposed into CH_3NH_3I and PbI_2.[45,53] The $CH_3NH_3PbI_3$ films deposited with AgAl and Ag films were exposed to saturated water vapor pressure at room temperature, as shown in Figure 6. The $CH_3NH_3PbI_3$ films

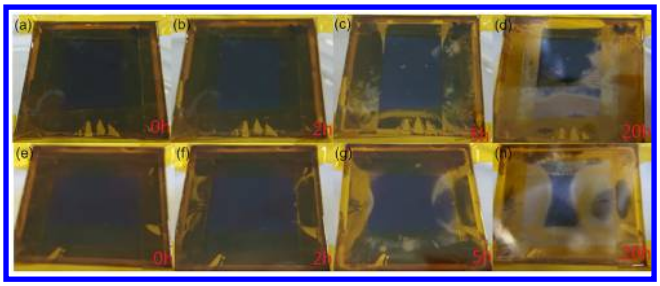

Figure 6. Evolutional process of $CH_3NH_3PbI_3$ films deposited with AgAl films (a–d) and Ag films (e–h) exposed to saturated water vapor pressure at room temperature for 2 h (b, f), 5 h (c, g) and 20 h (d, h).

deposited with Ag film compared to AgAl is more quickly varied from dark brown to yellow after exposing water vapor for 5 h, suggesting that AgAl films have superior capability of blocking moisture, which helps to improve the stability of cells. Therefore, formation of AlO_x in the AgAl electrode can also improve the capability of blocking moisture, which delays the deterioration of cell interfaces, including the ZnO/ITO interface, and enhances the stability of cells.

4. CONCLUSIONS

The effect of different metal contacts of Ag, Al and AgAl on the performance of the inverted PSCs was analyzed. The cells with a AgAl electrode show the highest PCE and better stability compared to the structurally identical PSCs made with the Ag and Al top electrodes. Formation of an AlO_x interlayer between MoO_3 and AgAl benefits the performance of the PSCs in two ways: (1) to prevent the diffusion of Ag atoms into organic layer and (2) to increase the built-in potential across the active layer. The presence of AlO_x also assists in forming a thermally stable organic/anode contact to impede the moisture encroachment,[48] thereby improving the stability of the cells. In comparison with the conventional Ag and Al electrodes, our results suggest that AgAl alloy contact is the most favorable electrode for application in high performance PSCs.

■ ASSOCIATED CONTENT

Supporting Information

The Supporting Information is available free of charge on the ACS Publications website at DOI: 10.1021/acsami.5b10240.

Average PCE values of polymer solar cells with $Ag_{97}Al_3$ and $Ag_{92}Al_8$(8 wt % Al) top contacts, XPS spectra of LiF, and optical microscope images of AgAl and Ag films for adhesion (PDF).

■ AUTHOR INFORMATION

Corresponding Author

*X. Chen. E-mail: xhchen@phy.ecnu.edu.cn. Tel.:+86 21 62233676. Fax: +86 21 62234321.

Notes

The authors declare no competing financial interest.

■ ACKNOWLEDGMENTS

This work was supported by National Natural Science Foundation of China (grant Nos. 61275038, 61275037 and 11274119), Research Grants Council of Hong Kong, Project No. GRF12303114, Hong Kong Baptist University FRG2/14-15/081, and Shenzhen Peacock Project, KQTD20140630110339343.

■ REFERENCES

(1) Hoppe, H.; Sariciftci, N. S. Organic Solar Cells: An Overview. *J. Mater. Res.* **2004**, *19* (07), 1924–1945.
(2) Li, G.; Zhu, R.; Yang, Y. Polymer Solar Cells. *Nat. Photonics* **2012**, *6* (3), 153–161.
(3) He, Z.; Zhong, C.; Su, S.; Xu, M.; Wu, H.; Cao, Y. Enhanced Power-Conversion Efficiency in Polymer Solar Cells Using an Inverted Device Structure. *Nat. Photonics* **2012**, *6* (9), 593–597.
(4) Mayer, A. C.; Scully, S. R.; Hardin, B. E.; Rowell, M. W.; McGehee, M. D. Polymer-Based Solar Cells. *Mater. Today* **2007**, *10* (11), 28–33.
(5) Liao, S. H.; Jhuo, H. J.; Yeh, P. N.; Cheng, Y. S.; Li, Y. L.; Lee, Y. H.; Sharma, S.; Chen, S. A. Single Junction Inverted Polymer Solar Cell Reaching Power Conversion Efficiency 10.31% by Employing Dual-Doped Zinc Oxide Nano-Film as Cathode Interlayer. *Sci. Rep.* **2014**, *4*, 6813.
(6) He, Z.; Xiao, B.; Liu, F.; Wu, H.; Yang, Y.; Xiao, S.; Wang, C.; Russell, T. P.; Cao, Y. Single-Junction Polymer Solar Cells with High Efficiency and Photovoltage. *Nat. Photonics* **2015**, *9* (3), 174–179.
(7) Liu, Y.; Zhao, J.; Li, Z.; Mu, C.; Ma, W.; Hu, H.; Jiang, K.; Lin, H.; Ade, H.; Yan, H. Aggregation and Morphology Control Enables Multiple Cases of High-Efficiency Polymer Solar Cells. *Nat. Commun.* **2014**, *5*, 5293.
(8) Chen, J.-D.; Cui, C.; Li, Y.-Q.; Zhou, L.; Ou, Q.-D.; Li, C.; Li, Y.; Tang, J.-X. Single-Junction Polymer Solar Cells Exceeding 10% Power Conversion Efficiency. *Adv. Mater.* **2015**, *27* (6), 1035–1041.
(9) Yusoff, A. R. b. M.; Kim, D.; Kim, H. P.; Shneider, F. K.; da Silva, W. J.; Jang, J. A High Efficiency Solution Processed Polymer Inverted Triple-Junction Solar Cell Exhibiting a Power Conversion Efficiency of 11.83%. *Energy Environ. Sci.* **2015**, *8* (1), 303–316.
(10) Liu, H.; Wu, Z.; Hu, J.; Song, Q.; Wu, B.; Lam Tam, H.; Yang, Q.; Hong Choi, W.; Zhu, F. Efficient and Ultraviolet Durable Inverted Organic Solar Cells Based on an Aluminum-Doped Zinc Oxide Transparent Cathode. *Appl. Phys. Lett.* **2013**, *103* (4), 043309.

DOI: 10.1021/acsami.5b10240
ACS Appl. Mater. Interfaces 2016, 8, 3792–3799

(11) Zeng, W.; Yong, K. S.; Kam, Z. M.; Zhu, F.; Li, Y. Effect of Blend Layer Morphology on Performance of ZnPc:C60-Based Photovoltaic Cells. *Appl. Phys. Lett.* **2010**, *97* (13), 133304.
(12) Oklobia, O.; Shafai, T. S. A Quantitative Study of the Formation of PCBM Clusters Upon Thermal Annealing of P3HT/PCBM Bulk Heterojunction Solar Cell. *Sol. Energy Mater. Sol. Cells* **2013**, *117*, 1−8.
(13) Li, G.; Shrotriya, V.; Yao, Y.; Yang, Y. Investigation of Annealing Effects and Film Thickness Dependence of Polymer Solar Cells Based on Poly(3-hexylthiophene). *J. Appl. Phys.* **2005**, *98* (4), 043704.
(14) He, Z.; Zhong, C.; Huang, X.; Wong, W. Y.; Wu, H.; Chen, L.; Su, S.; Cao, Y. Simultaneous Enhancement of Open-Circuit Voltage, Short-Circuit Current Density, and Fill Factor in Polymer Solar Cells. *Adv. Mater.* **2011**, *23* (40), 4636−4643.
(15) Hau, S. K.; Yip, H.-L.; Acton, O.; Baek, N. S.; Ma, H.; Jen, A. K. Y. Interfacial Modification to Improve Inverted Polymer Solar Cells. *J. Mater. Chem.* **2008**, *18* (42), 5113.
(16) Lan, W.; Cui, Y.; Yang, Q.; Lo, M.-F.; Lee, C.-S.; Zhu, F. Broadband Light Absorption Enhancement in Moth's Eye Nanostructured Organic Solar Cells. *AIP Adv.* **2015**, *5* (5), 057164.
(17) Chen, X.; Zhao, C.; Rothberg, L.; Ng, M.-K. Plasmon Enhancement of Bulk Heterojunction Organic Photovoltaic Devices by Electrode Modification. *Appl. Phys. Lett.* **2008**, *93* (12), 123302.
(18) Lu, Z.; Chen, X.; Zhou, J.; Jiang, Z.; Huang, S.; Zhu, F.; Piao, X.; Sun, Z. Performance Enhancement in Inverted Polymer Solar Cells Incorporating Ultrathin Au and LiF Modified ZnO Electron Transporting Interlayer. *Org. Electron.* **2015**, *17*, 364−370.
(19) Wu, B.; Wu, Z.; Tam, H. L.; Zhu, F. Contrary Interfacial Exciton Dissociation at Metal/Organic Interface in Regular and Reverse Configuration Organic Solar Cells. *Appl. Phys. Lett.* **2014**, *105*, 103302.
(20) Chang, J.; Lin, Z.; Zhu, C.; Chi, C.; Zhang, J.; Wu, J. Solution-Processed LiF-Doped ZnO Films for High Performance Low Temperature Field Effect Transistors and Inverted Solar Cells. *ACS Appl. Mater. Interfaces* **2013**, *5* (14), 6687−6693.
(21) Xu, M. F.; Zhu, X. Z.; Shi, X. B.; Liang, J.; Jin, Y.; Wang, Z. K.; Liao, L. S. Plasmon Resonance Enhanced Optical Absorption in Inverted Polymer/Fullerene Solar Cells with Metal Nanoparticle-Doped Solution-Processable TiO2 Layer. *ACS Appl. Mater. Interfaces* **2013**, *5* (8), 2935−2942.
(22) Tan, K. S.; Chuang, M. K.; Chen, F. C.; Hsu, C. S. Solution-Processed Nanocomposites Containing Molybdenum Oxide and Gold Nanoparticles as Anode Buffer Layers in Plasmonic-Enhanced Organic Photovoltaic Devices. *ACS Appl. Mater. Interfaces* **2013**, *5* (23), 12419−12424.
(23) Hau, S. K.; Yip, H.-L.; Baek, N. S.; Zou, J.; O'Malley, K.; Jen, A. K. Y. Air-Stable Inverted Flexible Polymer Solar Cells Using Zinc Oxide Nanoparticles as an Electron Selective Layer. *Appl. Phys. Lett.* **2008**, *92* (25), 253301.
(24) White, M. S.; Olson, D. C.; Shaheen, S. E.; Kopidakis, N.; Ginley, D. S. Inverted Bulk-Heterojunction Organic Photovoltaic Device Using a Solution-Derived ZnO Underlayer. *Appl. Phys. Lett.* **2006**, *89* (14), 143517.
(25) Yang, T.; Cai, W.; Qin, D.; Wang, E.; Lan, L.; Gong, X.; Peng, J.; Cao, Y. Solution-Processed Zinc Oxide Thin Film as a Buffer Layer for Polymer Solar Cells with an Inverted Device Structure. *J. Phys. Chem. C* **2010**, *114*, 6849−6853.
(26) Kam, Z.; Yang, Q.; Wang, X.; Wu, B.; Zhu, F.; Zhang, J.; Wu, J. Enhanced Absorbance and Electron Collection in Inverted Organic Solar Cells: Optical Admittance and Transient Photocurrent Analyses. *Org. Electron.* **2014**, *15* (7), 1306−1311.
(27) Sun, Y.; Takacs, C. J.; Cowan, S. R.; Seo, J. H.; Gong, X.; Roy, A.; Heeger, A. J. Efficient, Air-Stable Bulk Heterojunction Polymer Solar Cells Using MoO(x) as The Anode Interfacial Layer. *Adv. Mater.* **2011**, *23* (19), 2226−2230.
(28) Li, G.; Chu, C. W.; Shrotriya, V.; Huang, J.; Yang, Y. Efficient Inverted Polymer Solar Cells. *Appl. Phys. Lett.* **2006**, *88* (25), 253503.
(29) Kyaw, A. K. K.; Sun, X. W.; Jiang, C. Y.; Lo, G. Q.; Zhao, D. W.; Kwong, D. L. An Inverted Organic Solar Cell Employing a Sol-Gel Derived ZnO Electron Selective Layer and Thermal Evaporated MoO3 Hole Selective Layer. *Appl. Phys. Lett.* **2008**, *93* (22), 221107.
(30) Ma, T.; Jiang, K.; Chen, S.; Hu, H.; Lin, H.; Li, Z.; Zhao, J.; Liu, Y.; Chang, Y.-M.; Hsiao, C.-C.; Yan, H. Efficient Low-Bandgap Polymer Solar Cells with High Open-Circuit Voltage and Good Stability. *Adv. Energy Mater.* **2015**, *5* (20), 1501282.
(31) Wang, W.; Schaffer, C. J.; Song, L.; Körstgens, V.; Pröller, S.; Indari, E. D.; Wang, T.; Abdelsamie, A.; Bernstorff, S.; Müller-Buschbaum, P. In Operando Morphology Investigation of Inverted Bulk Heterojunction Organic Solar Cells by GISAXS. *J. Mater. Chem. A* **2015**, *3* (16), 8324−8331.
(32) Cheng, Y. S.; Liao, S. H.; Li, Y. L.; Chen, S. A. Physically Adsorbed Fullerene Layer on Positively Charged Sites on Zinc Oxide Cathode Affords Efficiency Enhancement in Inverted Polymer Solar Cell. *ACS Appl. Mater. Interfaces* **2013**, *5* (14), 6665−6671.
(33) Hu, T.; Li, F.; Yuan, K.; Chen, Y. Efficiency and Air-Stability Improvement of Flexible Inverted Polymer Solar Cells Using ZnO/Poly(ethylene glycol) Hybrids as Cathode Buffer Layers. *ACS Appl. Mater. Interfaces* **2013**, *5* (12), 5763−5770.
(34) Zhu, F.; Chen, X.; Zhou, L.; Zhou, J.; Yang, J.; Huang, S.; Sun, Z. Dependence of the Performance of Inverted Polymer Solar Cells on Thickness of an Electron Selective ZnO Layer Deposited by Magnetron Sputtering. *Thin Solid Films* **2014**, *551*, 131−135.
(35) Chen, X.; Zhu, F.; Lu, Z.; Yang, J.; Huang, S.; Sun, Z. Efficiency Enhancement of Inverted Polymer Solar Cells Using Ionic Liquid-Functionalized Carbon Nanoparticles-Modified ZnO as Electron Selective Layer. *Nano-Micro Lett.* **2014**, *6* (1), 24−29.
(36) Zhu, F.; Chen, X.; Zhou, J.; Lu, Z.; Chen, Y.; Huang, S.; Sun, Z. Enhanced Efficiency of Inverted Polymer Solar Cells Using Two-Step Sputtered ZnO as Cathode Interfacial Layer. *Mater. Res. Express* **2014**, *1* (2), 025020.
(37) Chen, S.; Manders, J. R.; Tsang, S.-W.; So, F. Metal Oxides for Interface Engineering in Polymer Solar Cells. *J. Mater. Chem.* **2012**, *22* (46), 24202.
(38) Stubhan, T.; Ameri, T.; Salinas, M.; Krantz, J.; Machui, F.; Halik, M.; Brabec, C. J. High Shunt Resistance in Polymer Solar Cells Comprising a MoO3 Hole Extraction Layer Processed from Nanoparticle Suspension. *Appl. Phys. Lett.* **2011**, *98* (25), 253308.
(39) Chambon, S.; Derue, L.; Lahaye, M.; Pavageau, B.; Hirsch, L.; Wantz, G. MoO3 Thickness, Thermal Annealing and Solvent Annealing Effects on Inverted and Direct Polymer Photovoltaic Solar Cells. *Materials* **2012**, *5* (12), 2521−2536.
(40) Gao, J.; Perkins, C. L.; Luther, J. M.; Hanna, M. C.; Chen, H. Y.; Semonin, O. E.; Nozik, A. J.; Ellingson, R. J.; Beard, M. C. N-Type Transition Metal Oxide as a Hole Extraction Layer in PbS Quantum Dot Solar Cells. *Nano Lett.* **2011**, *11* (8), 3263−3266.
(41) Liu, J.; Shao, S.; Fang, G.; Meng, B.; Xie, Z.; Wang, L. High-Effciency Inverted Polymer Solar Cells with Transparent and Work-Function Tunable MoO3-Al Composite Film as Cathode Buffer layer. *Adv. Mater.* **2012**, *24*, 2774−2779.
(42) Gao, J.; Tu, C.; Liang, L.; Zhang, H.; Zhuge, F.; Wu, L.; Cao, H.; Yu, K. Silver Nanoparticles with an Armor Layer Embedded in the Alumina Matrix to Form Nanocermet Thin Films with Sound Thermal Stability. *ACS Appl. Mater. Interfaces* **2014**, *6* (14), 11550−11557.
(43) Zhang, S. T.; Zhou, Y. C.; Zhao, J. M.; Zhan, Y. Q.; Wang, Z. J.; Wu, Y.; Ding, X. M.; Hou, X. Y. Role of Hole Playing in Improving Performance of Organic Light-Emitting Devices with an Al2O3 Layer Inserted at the Cathode-Organic Interface. *Appl. Phys. Lett.* **2006**, *89* (4), 043502.
(44) Kim, J.-Y.; Na, S.-I.; Ha, G.-Y.; Kwon, M.-K.; Park, I.-K.; Lim, J.-H.; Park, S.-J.; Kim, M.-H.; Choi, D.; Min, K. Thermally Stable and Highly Reflective AgAl Alloy for Enhancing Light Extraction Efficiency in GaN Light-Emitting Diodes. *Appl. Phys. Lett.* **2006**, *88* (4), 043507.
(45) Jiang, Z.; Chen, X.; Lin, X.; Jia, X.; Wang, J.; Pan, L.; Huang, S.; Zhu, F.; Sun, Z. Amazing Stable Open-Circuit Voltage in Perovskite Solar Cells Using AgAl Alloy Electrode. *Sol. Energy Mater. Sol. Cells* **2016**, *146*, 35−43.
(46) Luo, Y.; Chen, X.; Zhang, C.; Li, J.; Shi, J.; Sun, Z.; Wang, Z.; Huang, S. AgAl Alloy Electrode for Efficient Perovskite Solar Cells. *RSC Adv.* **2015**, *5* (69), 56037−56044.

DOI: 10.1021/acsami.5b10240
ACS Appl. Mater. Interfaces 2016, 8, 3792−3799

(47) Shao, S.; Zheng, K.; Pullerits, T.; Zhang, F. Enhanced Performance of Inverted Polymer Solar Cells by Using Poly(ethylene oxide)-Modified ZnO as an Electron Transport Layer. *ACS Appl. Mater. Interfaces* **2013**, *5* (2), 380−385.
(48) Wang, X.; Xinxin Zhao, C.; Xu, G.; Chen, Z.-K.; Zhu, F. Degradation Mechanisms in Organic Solar Cells: Localized Moisture Encroachment and Cathode Reaction. *Sol. Energy Mater. Sol. Cells* **2012**, *104*, 1−6.
(49) Kim, H. S.; Lee, H.; Jeon, P. E.; Jeong, K.; Lee, J. H.; Yi, Y. Revised Hole Injection Mechanism of a Thin LiF Layer Introduced Between Pentacene and an Indium Tin Oxide Anode. *J. Appl. Phys.* **2010**, *108* (5), 053701.
(50) Lu, L.; Luo, Z.; Xu, T.; Yu, L. Cooperative Plasmonic Effect of Ag and Au Nanoparticles on Enhancing Performance of Polymer Solar Cells. *Nano Lett.* **2013**, *13* (1), 59−64.
(51) Tu, C. J.; Gao, J. H.; Hui, S.; Lou, D.; Zhang, H. L.; Liang, L. Y.; Jin, A. P.; Zou, Y. S.; Cao, H. T. Alloyed Nanoparticle-Embedded Alumina Nanocermet Film: A New Attempt to Improve the Thermotolerance. *Appl. Surf. Sci.* **2015**, *331*, 285−291.
(52) Sugawara, K.; Kawamura, M.; Abe, Y.; Sasaki, K. Comparison of the Agglomeration Behavior of Ag(Al) Films and Ag(Au) Films. *Microelectron. Eng.* **2007**, *84* (11), 2476−2480.
(53) Niu, G.; Li, W.; Meng, F.; Wang, L.; Dong, H.; Qiu, Y. Study on the Stability of CH3NH3PbI3 Films and the Effect of Post-Modification by Aluminum Oxide in All-Solid-State Hybrid Solar Cells. *J. Mater. Chem. A* **2014**, *2* (3), 705−710.

DOI: 10.1021/acsami.5b10240
ACS Appl. Mater. Interfaces 2016, 8, 3792−3799